Label-free detection of protein-protein interactions using a calmodulin-modified nanowire transistor

Tsung-Wu Lin[a,b], Po-Jen Hsieh[a,b], Chih-Lung Lin[c], Yi-Ya Fang[c], Jia-Xun Yang[a,b], Chia-Chang Tsai[a,b], Pei-Ling Chiang[a,b], Chien-Yuan Pan[c,1], and Yit-Tsong Chen[a,b,1]

[a]Institute of Atomic and Molecular Sciences, Academia Sinica, P.O. Box 23-166, Taipei 106, Taiwan; [b]Department of Chemistry, National Taiwan University, No. 1, Sec. 4, Roosevelt Road, Taipei 106, Taiwan; and [c]Institute of Zoology and Department of Life Science, National Taiwan University, No. 1, Sec. 4, Roosevelt Road, Taipei 106, Taiwan

Edited by Charles Lieber, Harvard University, Cambridge, MA, and approved November 30, 2009 (received for review September 10, 2009)

In this study, we describe a highly sensitive and reusable silicon nanowire field-effect transistor for the detection of protein-protein interactions. This reusable device was made possible by the reversible association of glutathione S-transferase-tagged calmodulin with a glutathione modified transistor. The calmodulin-modified transistor exhibited selective electrical responses to Ca^{2+} ($\geq 1\ \mu M$) and purified cardiac troponin I (~7 nM); the change in conductivity displayed a linear dependence on the concentration of troponin I in a range from 10 nM to 1 μM. These results are consistent with the previously reported concentration range in which the dissociation constant for the troponin I-calmodulin complex was determined. The minimum concentration of Ca^{2+} required to activate calmodulin was determined to be 1 μM. We have also successfully demonstrated that the N-type Ca^{2+} channels, expressed by cultured 293T cells, can be recognized specifically by the calmodulin-modified nanowire transistor. This sensitive nanowire transistor can serve as a high-throughput biosensor and can also substitute for immunoprecipitation methods used in the identification of interacting proteins.

calcium ion | glutathione S-transfrease | N-type calcium channel | silicon nanowire field-effect transistor

In the postgenomic era, the understanding of protein functions and interactions is the key to unraveling the many puzzles that exist in the life sciences. Techniques such as fluorescence resonance energy transfer (1, 2), coimmunoprecipitation, and surface plasmon resonance (SPR) have been developed to analyze protein-protein interactions (3). With the exception of SPR, these techniques have the disadvantages of requiring fluorescence labeling and/or protein-specific antibodies, necessitating large amounts of sample, and/or being very time-consuming. Comparing SPR with silicon nanowire field-effect transistor (SiNW-FET)-based methods, Bunimovich et al. suggested that the sensitivity of the latter for DNA detection is 100 times higher (4).

In recent years, SiNW-FET has attracted great attention because it is an ideal biosensor with high selectivity and sensitivity, real-time response, and allows for label-free detection (5). SiNW-FET has been demonstrated to be capable of detecting a variety of analytes, such as metal ions (6, 7), DNA (4, 8), viruses (9), and neuronal propagation signals (10). Previous applications of SiNW-FET as a biosensor have mainly been based on antigen-antibody interactions. Lieber's group has shown that SiNW-FET modified with a specific antibody against a prostate cancer marker can detect the antigen in donkey serum at a concentration of 0.9 pg/mL (11). In similar experiments, we have used a carbon nanotube-configured FET to detect chromogranin A, a cancer marker for neuroendocrine neoplasia, at the subnanomolar level (12). However, monitoring various types of protein-protein interactions can be challenging for such FET-based sensors because these interactions have association constants of $K_a \sim 10^6$–$10^9\ M^{-1}$ that are weaker than antibody-antigen interactions with association constants of $K_a > 10^9\ M^{-1}$ (13).

Calmodulin (CaM) is an acidic protein consisting of approximately 148 amino acids and four EF-hand motifs that are responsible for Ca^{2+} binding when intracellular Ca^{2+} concentrations are elevated from a resting submicromolar level to a concentration one or two orders of magnitude higher (14). Ca^{2+}-bound CaM activates various proteins that modulate physiological activities, including gene transcription, muscle contraction, and neurotransmitter release (15). In the current study, we show that CaM-modified SiNW-FET (referred to as CaM/SiNW-FET) can be used to detect Ca^{2+} and CaM-interacting proteins. Becuase the SiNW is boron-doped, the binding of cardiac troponin I (TnI) to CaM/SiNW-FET decreased the conductance of the p-type FET sensor in a dose-dependent manner. The threshold $[Ca^{2+}]$ needed for the interaction between TnI and CaM was determined to be at the micromolar level. Furthermore, the N-type voltage-gated Ca^{2+} channel (VGCC) present in the membrane fraction prepared from transfected cells was recognized by CaM/SiNW-FET. These results suggest that there is great potential for the application of SiNW-FET as a high-throughput detector to identify interacting proteins in physiologically relevant environments.

Results and Discussion

The reversible association of CaM onto the SiNW-FET surface was based on a method that we previously developed (16). We took advantage of the reversible association-dissociation between glutathione (GSH) and glutathione S-transferase (GST)-tagged CaM (referred to as CaM-GST) to develop a CaM-modified nanowire transistor. Fig. 1 schematically illustrates the implantation of reactive GSH onto a SiNW-FET surface (referred to as GSH/SiNW-FET). As illustrated, the association of CaM-GST with the GSH/SiNW-FET results in the formation of CaM/SiNW-FET, which can then detect various target proteins via CaM-protein interactions. Upon dissociation of the CaM/SiNW-FET complex, the device returns to its original status (GSH/SiNW-FET). This unique strategy allows the sensitive nanowire transistor to serve as a reusable and high-throughput biosensor for the rapid screening of potential CaM-binding proteins.

As shown in Fig. 2*A*, a microscopic fluorescence imaging technique was used to confirm the successful association of GST with GSH-modified micropatterns. Using a fluorescein isothiocyanate (FITC)-labeled antibody against GST, we observed green fluorescence radiating from the square micropatterns anchored to GST, indicating the successful association of GST with a GSH-modified substrate (experimental details are provided in the

Author contributions: T.-W.L., C.-Y.P., and Y.-T.C. designed research; T.-W.L., P.-J.H., C.-L.L., Y.-Y.F., and J.-X.Y. performed research; T.-W.L., P.-J.H., C.-Y.P., and Y.-T.C. analyzed data; T.-W.L., C.-Y.P., and Y.-T.C. wrote the paper; and C.-L.L., Y.-Y.F., C.-C.T., and P.-L.C. contributed new reagents/analytic tools.

The authors declare no conflict of interest.

This article is a PNAS Direct Submission.

[1]To whom correspondence may be addressed. E-mail: ytcchem@ntu.edu.tw or cypan@ntu.edu.tw

This article contains supporting information online at www.pnas.org/cgi/content/full/0910243107/DCSupplemental.

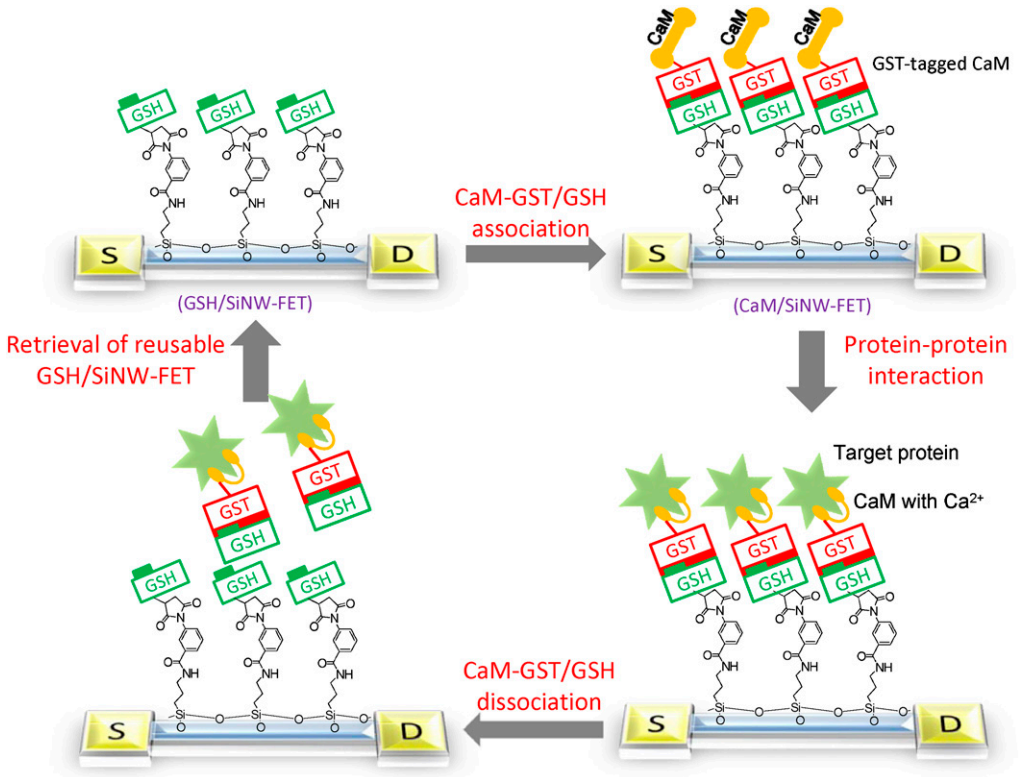

Fig. 1. Schematic of the experimental approach. The strategy used in this study included the association of CaM-GST with a GSH/SiNW-FET to form the CaM/SiNW-FET complex, the subsequent detection of interacting proteins, and the removal of bound proteins via the dissociation of GSH-GST with 1 mM GSH washing solution.

Supporting Information). To further prove the reversible association between GSH-GST on the SiNW-FET sensor fabricated with a bottom-up technique, we performed real-time electrical measurements of GST binding using a GSH/SiNW-FET. Given the effects of electrolytes on the electrical measurements taken by a SiNW-FET, we generally used phosphate solution ($0.1 \times$ PS, consisting of 0.76 mM Na_2HPO_4 and 0.24 mM NaH_2PO_4 at pH 7.4) as a buffer in all of the sensing experiments, of which the corresponding Debye screening length (λ_D) is 6.1 nm. The electrical measurements under such a solution environment should effectively reflect the binding of interacting proteins to CaM-GST that was estimated to be ~5.6 nm distant from the surface of the SiNW-FET (17, 18). As shown in Fig. 2*B*, the electrical conductance was approximately 398 nS when the GSH/SiNW-FET was incubated with GSH solution (1 mM in $0.1 \times$ PS, pH 4.5) and increased to approximately 403 nS after washing off the GSH with $0.1 \times$ PS at pH 7.4. This increase in conductance was mainly attributed to the deprotonation of the silanol groups on the SiNW surface due to the pH variation (5), as demonstrated in the *SI Text*. The introduction of GST (5 μM in $0.1 \times$ PS, pH 7.4) caused an appreciable increase in conductance to approximately 406 nS that was the result of a gating effect generated by the negatively charged GST (pI ~ 6.72) at pH 7.4. After the removal of GST by washing with 1 mM GSH and reintroducing $0.1 \times$ PS, the conductance returned to 402 nS, similar to the conductance level of $0.1 \times$ PS at the beginning of the experiment. Repeating the association of GST with the GSH/SiNW-FET changed the conductance to the same level, suggesting the reusability of this sensor in detecting bound molecules.

Fig. 2*C* shows the increase in conductance of the p-type GSH/SiNW-FET after the addition of CaM-GST in a Ca^{2+}-free buffer. The increase in conductance was caused by binding of the negatively charged CaM (pI ~ 4) to the GSH/SiNW-FET at pH 7.4 (19). By comparison, a bare SiNW-FET (without any surface modification) showed no response to CaM-GST (Fig. S2B), which indicates that the change in conductance (ΔG) of the GSH/SiNW-FET in Fig. 2*C* was induced by the specific binding of CaM-GST.

It was noted that a trace amount of metal ions present in the buffer might interfere with the sensing of ions by the CaM/SiNW-FET (Fig. S3). To examine how binding of various metal ions affects the conductance of CaM/SiNW-FET, a free 10^{-4} M metal ion solution was prepared in $1 \times$ PS and supplemented with 0.5 mM ethylenediaminetetraacetic acid (EDTA) ($\lambda_D \sim 1.9$ nm, pH 7.1) (20). Fig. 2*D* demonstrates that the conductance of the CaM/SiNW-FET was not affected by K^+ but decreased by 0.3% and 1% with Al^{3+} and Ca^{2+}, respectively. The observed decreases in conductance result from the binding of cations to the p-type CaM/SiNW-FET (5). The device showed no electrical response to K^+, likely due to the much greater mean dissociation constant of CaM for K^+ than for Ca^{2+} (approximately two orders of magnitude greater) (21). Although the binding affinities of CaM to Al^{3+} and Ca^{2+} are comparable (22), Al^{3+} caused only a small decrease in conductance in the CaM/SiNW-FET. This small conductance change might stem from the fact that the conformation of GST-CaM is slightly altered from the wild-type CaM, leading the former to have a weaker binding affinity for Al^{3+}. In a control experiment, if the GSH/SiNW-FET was associated with GST only (referred to as GST/SiNW-FET) without tagged CaM, the GST/SiNW-FET showed no electrical response to the Ca^{2+}-containing solution (Fig. S4). This indicated that CaM is essential for Ca^{2+} sensing. Collectively, these results demonstrated that the CaM/SiNW-FET exhibits high specificity for Ca^{2+}.

TnI is known to bind CaM in a Ca^{2+}-dependent manner and has been used as a diagnostic marker of myocardial infarction (23–25). Fig. 3*A* shows the detection of TnI by the CaM/SiNW-FET in the presence of Ca^{2+}. The decrease in conductance in the CaM/SiNW-FET after addition of TnI originated from the

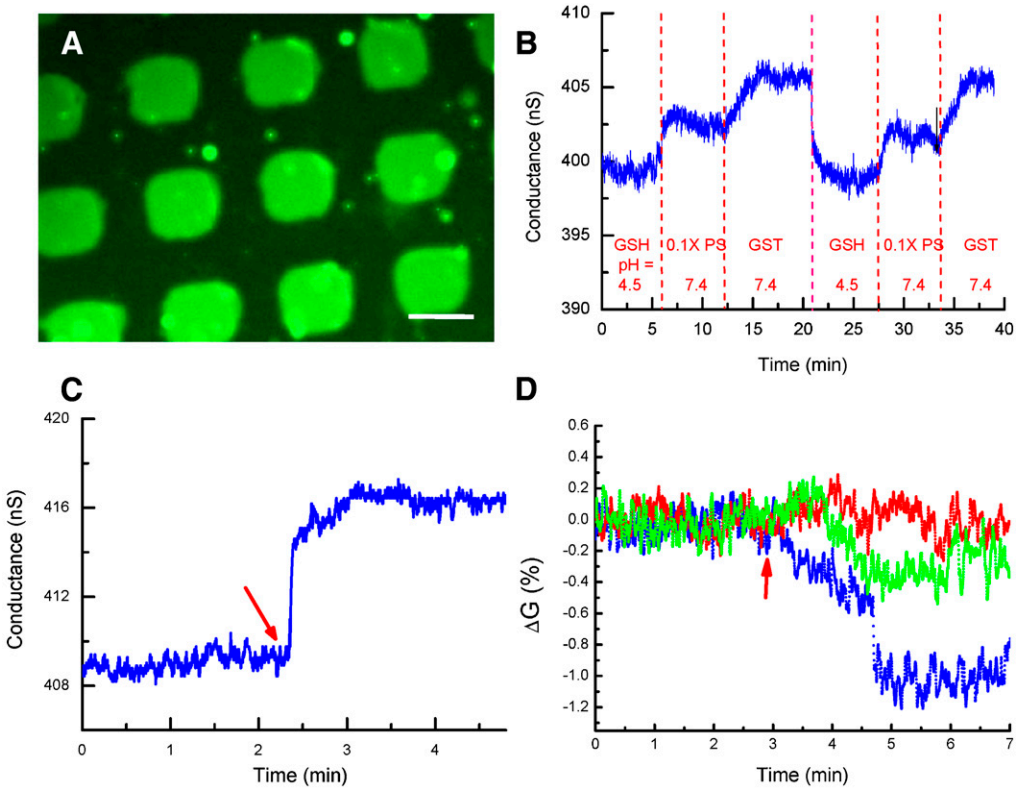

Fig. 2. Reversible association of CaM on a SiNW-FET. (*A*) Fluorescence image of FITC-labeled anti-GST antibody bound to anchored GST on GSH-modified micropatterns. The scale bar represents 50 μm. (*B*) Real-time electrical responses for the association and dissociation of GST with a GSH/SiNW-FET. The concentrations and pH values for the sample solutions were GSH (1 mM in 0.1 × PS, pH 4.5), 0.1 × PS at pH 7.4, and GST (5 μM in 0.1 × PS, pH 7.4). (*C*) Real-time electrical measurements for the association of 400 nM CaM-GST with the GSH/SiNW-FET in 0.1 × PS solution supplemented with 0.5 mM EDTA ($\lambda_D = 4.2$ nm). The *arrow* indicates the arrival of the CaM-GST solution. (*D*) Real-time detection of the binding of K^+ (*red*), Al^{3+} (*green*), and Ca^{2+} (*blue*) to the CaM/SiNW-FET. The *arrow* indicates the arrival of the appropriate ion solution.

positively charged TnI (pI ~ 9.3) at pH 7.4 (26). To ensure the specificity of this interaction, we conducted several control tests. The top graph in Fig. 3*B* demonstrates that the CaM/SiNW-FET had no electrical response to avidin, a positively charged protein with a pI of ~9.5 (27). Furthermore, boiled TnI did not generate a measurable ΔG in the CaM/SiNW-FET (Fig. 3*B*, *middle graph*), whereas the same device was able to detect TnI at a concentration as low as 7 nM (Fig. 3*B*, *yellow region*). Keller et al. (24) reported that the binding affinity of TnI to CaM is enhanced ~4, 500-fold in the presence of Ca^{2+}. Here, we show that no measurable ΔG in the CaM/SiNW-FET was observed upon the addition of 231 nM TnI dissolved in a Ca^{2+}-free buffer (Fig. 3*B*, *bottom graph*). In contrast, we found that 231 nM TnI readily bound to CaM in the presence of Ca^{2+} (Fig. 3*A*). Moreover, bound TnI could be washed off with Ca^{2+}-free buffer; as a result, the reversible binding of TnI to CaM allowed us to use a single SiNW-FET device to monitor the ΔG as a function of TnI concentration. Figure 3*C* shows that the ΔG of the CaM/SiNW-FET increased with the log of TnI concentration, and this concentration dependence was linear in the range of 10^{-8}–10^{-6} M. This linear dependence range closely overlapped with a previously reported concentration range where the dissociation constant for the TnI-CaM complex was estimated (25). The same device also showed no response to TnI dissolved in EDTA due to the weak affinity of TnI for CaM in the absence of Ca^{2+}. This concentration range is consistent with the physiological concentration change, again, demonstrating the potential of applying the SiNW-FET as a biosensor to detect physiological interactions.

The $[Ca^{2+}]$ needed to activate the TnI-CaM interaction is very important in understanding the interaction under physiological conditions. However, to the best of our knowledge, there are no reports that have investigated the quantitative dependence of this interaction on Ca^{2+}. Fig. 3*D* shows that, whereas no measurable ΔG was observed in the CaM/SiNW-FET when TnI was dissolved in buffers containing 10^{-8}- and 10^{-7} M-free Ca^{2+} (*blue* and *red curves*, resp.), the ΔG became significant as the $[Ca^{2+}]$ increased. The minimal measurable ΔG was detected at $[Ca^{2+}] = 10^{-6}$ M (Fig. 3*D*, *green curve*, signal-to-noise ratio ≥ 3). When we replaced Ca^{2+} (10^{-6} M) with Ba^{2+} (10^{-4} M), no measurable electrical response was observed (Fig. 3*D*, *black curve*), indicating that Ba^{2+} could not substitute for Ca^{2+} in the activation of protein-protein interactions. This outcome can be attributed to the fact that Ba^{2+} has significantly lower affinity towards CaM that weakens the tendency of CaM to undergo conformational changes (28). Although the $[Ba^{2+}]$ used in the sensing experiment was 100 times higher than that of $[Ca^{2+}]$, it was still not sufficient to trigger the association of TnI with CaM. These results are in agreement with previous studies showing that the $[Ba^{2+}]$ required for CaM activation is approximately 200-fold higher than that for $[Ca^{2+}]$ (29, 30). Overall, these electrical measurements suggested that the SiNW-FET can be applied for the investigation of the detailed mechanisms of protein-protein interactions.

The central focus of this study is the practical use of the SiNW-FET for probing target proteins present in a biochemical system. N-type VGCCs located at the plasma membrane mediate the entry of Ca^{2+} into cells in response to membrane depolarization. The Ca^{2+}-dependent inactivation (CDI) of several Ca^{2+} channel subtypes has been suggested to be mediated by the binding of CaM to the C-termini of these channels (31). To characterize the effect of CaM on N-type VGCC CDI, rat CaM was cloned and co-expressed with the N-type VGCC in 293T cells. Transfected cells were voltage-clamped in a whole-cell configuration

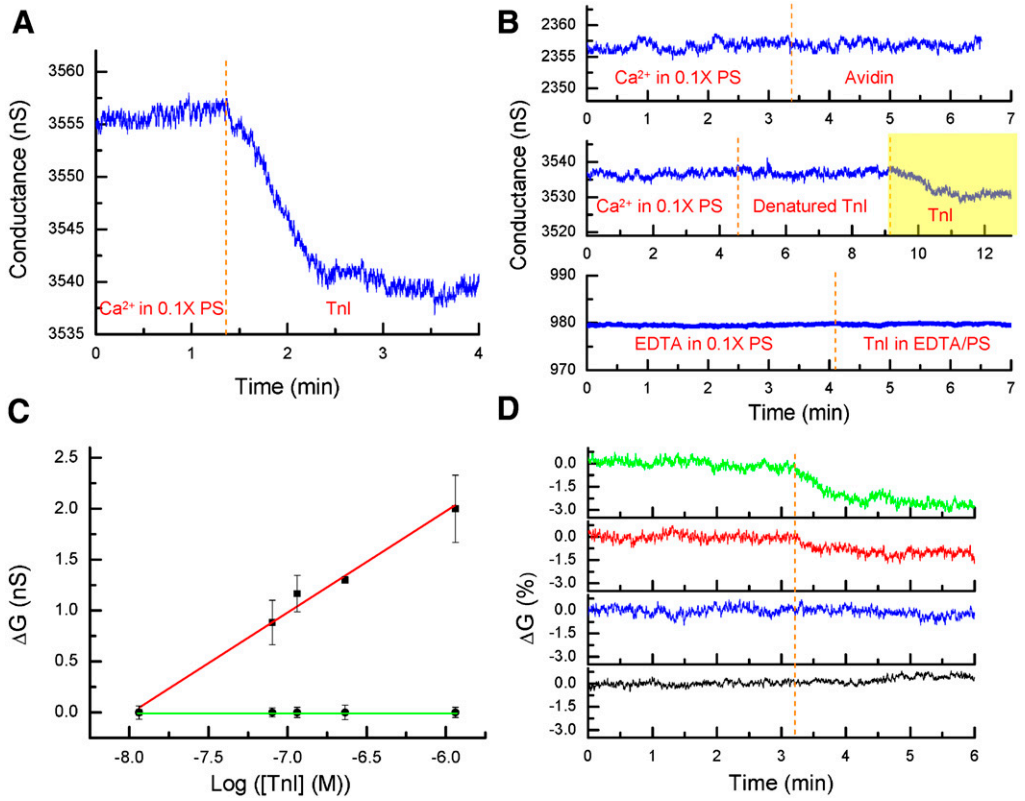

Fig. 3. Detection of cardiac TnI by the CaM/SiNW-FET. (*A*) Real-time detection of the binding of 231 nM TnI to a CaM/SiNW-FET in 0.1 × PS supplemented with 10^{-4} M Ca^{2+}. (*B*) Three control experiments were conducted separately with the same CaM/SiNW-FET. *Top*, *middle*, and *bottom graphs* correspond to the detection of 231 nM avidin in 0.1 × PS supplemented with 10^{-4} M Ca^{2+}, 231 nM boiled TnI in 0.1 × PS supplemented with 10^{-4} M Ca^{2+}, and 231 nM TnI in 0.1 × PS supplemented with 0.5 mM EDTA, resp. (*C*) Plot of Δ*G* vs. the log of [TnI]. Different concentrations of TnI were added to 0.1 × PS supplemented with 10^{-4} M Ca^{2+} (■) or 0.5 mM EDTA (•). Electrical measurements were conducted with the same CaM/SiNW-FET device, and each data point represents the mean ±SEM of at least three measurements. The *red line* represents a linear fit to the five concentration data points (correlation coefficient = 0.987). (*D*) Real-time electrical measurements for the [Ca^{2+}] required to activate CaM where the binding of 231 nM TnI to CaM/SiNW-FET was detected in free Ba^{2+} at 10^{-4} M (*black*), free Ca^{2+} at 10^{-8} M (*blue*), free Ca^{2+} at 10^{-7} M (*red*), and free Ca^{2+} at 10^{-6} M (*green*). The dotted line indicates the arrival of the ion solutions. To prepare free Ca^{2+} solutions at 10^{-8}, 10^{-7}, and 10^{-6} M, total Ca^{2+} levels were calculated using Maxchelator software (http://maxchelator.stanford.edu/) and added to 0.1 × PS supplemented with 0.5 mM EDTA. These sensing experiments were performed using three different CaM/SiNW-FET devices with similar electric transport properties.

at −70 mV and depolarized to +20 mV to evoke Ca^{2+} currents. Fig. 4*A* shows that the representative current in cells expressing CaM decreased to ∼15% of the maximal current at the end of depolarization. On the contrary, this decline was ∼66% in cells expressing CaM_{1234}, a mutant of CaM that lacks the ability to bind Ca^{2+} (Fig. 4*B*). As shown in Fig. 4*C*, the mean level of inactivation was 13.3 ± 2.3% ($n = 7$) in cells expressing wild-type CaM and 40.7 ± 8.1% ($n = 5$) in cells expressing CaM_{1234}. These results suggested that CaM is essential for the CDI of N-type VGCCs. However, it is not clear whether N-type VGCCs directly interact with CaM.

Fig. 4*D* schematically illustrates how N-type VGCCs can be detected under physiological conditions with the CaM/SiNW-FET. Briefly, transfected 293T cells resuspended in the phosphate buffered saline (1 × PBS, consisting of 137 mM NaCl, 2.7 mM KCl, 10 mM Na_2HPO_4, and 2 mM KH_2PO_4 at pH 7.4) were sonicated and then centrifuged to isolate the membrane fractions. After being resuspended and diluted in 0.1 × PS, the membrane fractions (1.7 μg/μL) were delivered through a polydimethylsiloxane (PDMS) microfluidic channel onto the CaM/SiNW-FET surface, where N-type VGCCs bound to the immobilized CaM. The exact concentration of VGCCs was difficult to estimate; however, Fig. 4*E* shows that the CaM/SiNW-FET was able to detect N-type VGCCs in the presence of Ca^{2+}. The decrease in conductance after the addition of cell lysate containing N-type VGCCs was caused by the presence of positively charged Ca^{2+} channels at pH 7.4 (pI ∼ 8.79, University of California, San Diego-Nature Signaling Gateway Molecules Pages, Molecular pages ID: A000444). The binding of N-type VGCCs to the CaM-modified Si substrate was also verified by immunostaining (Fig. S5). Comparatively, in the absence of Ca^{2+} (Fig. 4*F*), the Ca^{2+} channel lysate also caused an appreciable decrease in the conductance of the CaM/SiNW-FET. It has been reported that the association of CaM with a peptide covering the IQ domain at the C-terminal of the N-type VGCC occurs in the presence or absence of Ca^{2+} (32) that is consistent with our electrical measurements. Furthermore, the addition of membrane lysate without the α1b subunit of the Ca^{2+} channel (Fig. 4*G*, *top graph*) did not cause any significant Δ*G*, indicating that the conductance of CaM/SiNW-FET is Ca^{2+} channel-specific. Moreover, a GST/SiNW-FET (without tagged CaM) had no electrical response to lysate containing N-type VGCCs (Fig. 4*G*, *bottom graph*), clearly indicating that CaM was essential for the detection of N-type VGCCs. These results once more supported the application of the SiNW-FET as a biosensor for the detection of protein-protein interactions under physiological conditions.

Conclusions

In summary, we have demonstrated that the reversible association of CaM onto a SiNW-FET surface through the association-dissociation of GSH-GST allowed us to utilize a reusable sensor to detect various protein-protein interactions from either purified protein or crude cell extracts. In the presence of Ca^{2+},

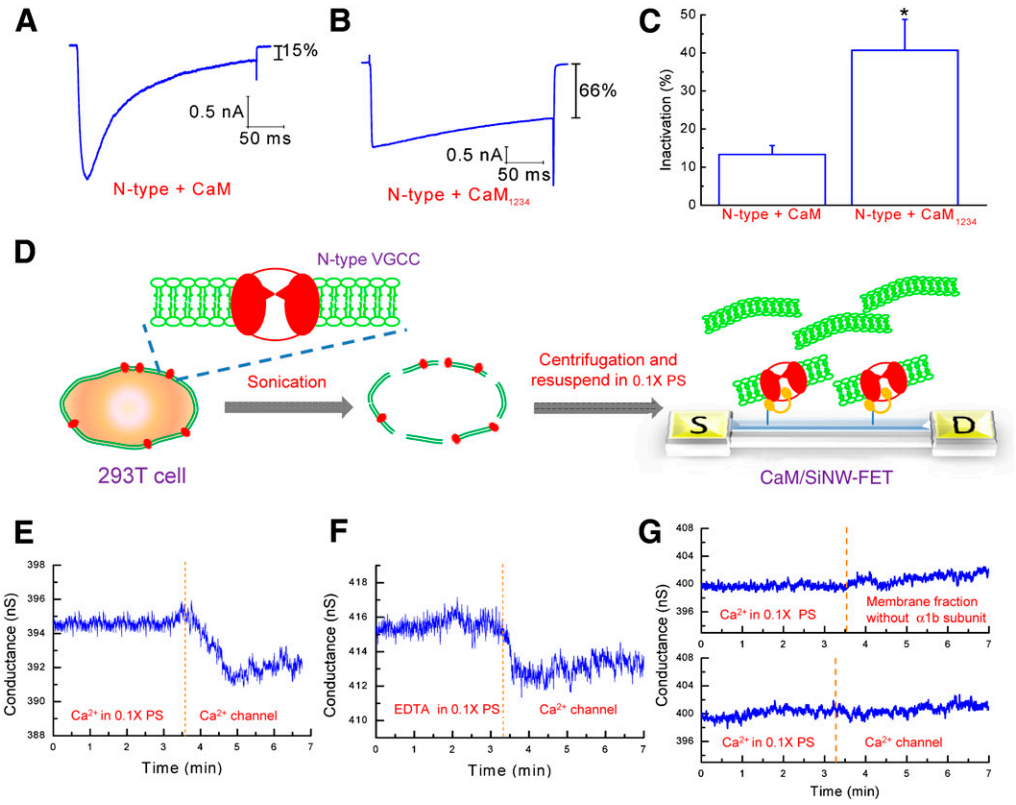

Fig. 4. Detection of N-type Ca^{2+} channels using the CaM/SiNW-FET. (*A-C*) Ca^{2+} currents in transfected 293T cells were recorded using a whole-cell patch configuration. The cells were voltage-clamped at −70 mV and depolarized to +20 mV for 250 ms to activate N-type VGCCs. Representative current traces from cells co-expressing N-type VGCCs with (*A*) CaM and (*B*) CaM_{1234} (a Ca^{2+} binding deficient mutant) are shown. Inactivation was obtained by normalizing the average currents between the 225 and 250 ms to the peak current during depolarization. (*C*) The bar graph depicts the average normalized inactivation values for cells expressing the different CaM constructs. The data represent the mean ±SEM. The sample numbers for N-type + CaM and N-type + CaM_{1234} are seven and five, resp. The * indicates a *p*-value of <0.05, as obtained by the student's *t*-test. (*D*) Scheme for the detection of membrane fractions containing N-type VGCCs by CaM/SiNW-FET. (*E-F*) The electrical measurements represent the real-time detection of the binding of an N-type Ca^{2+} channel to the CaM/SiNW-FET in 0.1 × PS supplemented with (*E*) 10^{-4} M Ca^{2+} or (*F*) 0.5 mM EDTA. (*G*) Two control experiments were conducted separately. (*Top graph*) Sensing of the membrane fraction without the α1b subunit by the CaM/SiNW-FET in 0.1 × PS supplemented with 10^{-4} M Ca^{2+}. (*Bottom graph*) Sensing of a Ca^{2+} channel with a GST/SiNW-FET in 0.1 × PS supplemented with 10^{-4} M Ca^{2+}. The protein concentration for the sensing experiments was 1.7 μg/μL.

the interaction between TnI with CaM could be detected by CaM/SiNW-FETs, and the detection limit of TnI was as low as 7 nM. Furthermore, the ΔG of CaM/SiNW-FETs increased linearly with the log of [TnI] over a range of 10^{-8}–10^{-6} M. Moreover, CaM/SiNW-FETs were also used to examine the detailed mechanisms of protein-protein interactions. A series of electrical measurements revealed that Ca^{2+} was pivotal to activate the interaction between CaM and TnI; the minimum [Ca^{2+}] required for this activation was approximately 10^{-6} M, which is within the physiological concentration. Finally, we have shown that CaM/SiNW-FETs can specifically recognize N-type VGCCs present in cell extracts with or without Ca^{2+}. Our results demonstrated that SiNW-FETs can serve as a substitute for immunoprecipitation methods and can function as high-throughput biosensors for the rapid screening of protein-protein interactions under physiological conditions.

Materials and Methods

Solution Preparation. Phosphate buffered saline (1 × PBS, pH 7.4) consisted of 137 mM NaCl, 2.7 mM KCl, 10 mM Na_2HPO_4, and 2 mM KH_2PO_4. Phosphate solution (1 × PS, pH 7.4) consisted of 7.6 mM Na_2HPO_4 and 2.4 mM NaH_2PO_4. The pH of all solutions was adjusted using NaOH. Hank's Balanced Salt Solution (HBSS), Dulbecco's modified Eagle's medium, and all other reagents for cell culture were purchased from Invitrogen.

To record Ca^{2+} currents, cells were incubated in N-methyl-D-glucamine (NMG) solution (130 mM NMG, 2 mM KCl, 5 mM $CaCl_2$, 1 mM $MgCl_2$, 5.6 mM glucose, and 10 mM HEPES at pH 7.3) and whole-cell patched with a Cs^+-containing pipette solution (130 mM Cs-aspartate, 20 mM KCl, 1 mM $MgCl_2$, 0.1 mM EGTA, 3 mM Na_2ATP, 0.1 mM Na_2GTP, and 20 mM HEPES at pH 7.3).

Reversible Surface Association. Before surface modification, the SiNW-FET chip (Fig. S6) was cleaned with oxygen plasma (30 W and 50 sccm O_2 for 60 s). Self-assembled silane monolayers were formed by immersing the chip in an ethanol solution supplemented with 3% 3-(aminopropyl)trimethoxysilane (APTMS, Acros) for 30 min. The chip was then washed with ethanol, blow-dried in a stream of nitrogen gas (N_2), and heated at 120 °C for 10 min. Subsequently, the silanized chip was immersed for 30 min in a 1:9 (v/v) solution of dimethyl sulfoxide (DMSO) and 1 × PBS containing 1 mM 3-maleimidobenzoic acid N-hydroxysuccinimide ester (MBS, Sigma). After MBS reacted with APTMS via the formation of an amide bond, the chip was rinsed with ethanol three times, blow-dried with N_2, and then immersed in 1 mM GSH solution (Sigma) for 30 min. GSH was dissolved in 1 × PBS containing 1 mM EDTA to promote the chelation of divalent metal ions and prevent the formation of disulfide bonds between sulfhydryl-containing reactants. After the sulfhydryl group of GSH bound to the maleimide group of MBS, the chip was washed with 1 × PBS and blow-dried with N_2. For the association of CaM to the GSH/SiNW-FET device, a 0.1 × PS solution containing 200 nM CaM-GST (Abnova) was pumped into a PDMS microfluidic channel (6.25 × 0.5 × 0.05 mm^3) that was designed to couple with the SiNW-FET device arrays through a syringe pump (KD Scientific, KD-101) at a flow rate of 0.3 mL/hr for 30 min.

Electrical Measurements. For protein sensing experiments, such as the detection of cardiac TnI (Abcam), the conductance of the CaM/SiNW-FET was measured at a source-drain voltage (V_{ds}) of 30 mV, a modulation frequency of 79 Hz, and a time constant of 100 ms using a detection system that combined a current preamplifier (DL Instrument, 1211) and a lock-in amplifier

(Stanford Research System, SR830). Furthermore, an Ag/AgCl electrode (BAS, MF2052) coupled to the PDMS microchannel was used as a solution gate and was kept at ground potential throughout the real-time electrical measurements to minimize noise in the system (4).

Electrophysiological Measurements. Cells were transferred into a recording chamber mounted on the stage of an inverted microscope and bathed in NMG solution at room temperature. Patch pipettes were pulled from thin-wall capillaries containing a filament (A-M Systems, Catalog 617000), using a two-stage microelectrode puller (Sutter, P-97), and were fire-polished with a microforge (Narishige, MF-830). Ionic currents were measured from patched cells using an EPC10 patch-clamp amplifier (HEKA GmbH) controlled by Pulse software (HEKA GmbH).

To measure Ca^{2+} currents, cells were incubated in NMG solution supplemented with 10 mM $CaCl_2$ and whole-cell voltage-clamped at −70 mV. The cells were depolarized to +20 mV for 250 ms. The average current values obtained during the 225 and 250 ms depolarizations were normalized to the peak inward current to represent inactivation.

Constructs and Molecular Biology. Plasmids for the bovine N-type Ca^{2+} channel (α1b) and its accessory subunits (β1 and $\alpha2\delta$) were generous gifts from Aaron P. Fox (University of Chicago) (33). Primers specific for CaM were designed according to the published CaM sequence and were used to amplify CaM from cDNA synthesized from purified rat total RNA by PCR. The amplified CaM product was subcloned into a pcDNA3.1 expression vector. To inactivate the Ca^{2+} binding ability of CaM, glutamate residues at positions 32, 68, 105, and 148 were mutated to glutamine.

Transfection of Human Embryonic Kidney 293T Cells. HEK 293T cells were maintained in Dulbecco's modified Eagle medium (Gibco), supplemented with 10% of fetal bovine serum, in a humidified incubator under 5% CO_2. For the transient expression of N-type Ca^{2+} channels and CaM in 293T cells, we used the Lipofectamine™ reagent (Invitrogen), according to the manufacture's instructions. A total of 2 μg of each plasmid (carrying the genes for CaM, α1b, β1, or $\alpha2\delta$) at a molar ratio of 1 : 1 was used to transfect 293T cells grown in a 35 mm dish. To verify transfection, 0.2 μg of pEGFP (Clontech) was added to the plasmid mixture. The transfected cells were incubated in a humidified CO_2 incubator for 2 d. Transfected cells with the lowest fluorescent GFP signal were selected for recording.

To isolate the membrane fraction, ~10^7 cells transfected with the α1b, β1, and $\alpha2\delta$ plasmids for 2 d were resuspended in 1 × PBS. As a control, α1b was omitted from the transfection mixture for a subset of cells. The sonicated cell suspension was first centrifuged at 1, 000 × *g* for 30 min, followed by collection of the supernatant. The supernatant was then centrifuged at 100, 000 × *g* for 2 hr, and the pellet was resuspended in 0.2 mL of 0.1 × PS. The extract was diluted with 0.1 × PS containing either no free Ca^{2+} or 0.1 mM free Ca^{2+}.

ACKNOWLEDGMENTS. We thank Dr. Shu-Ping Lin for her assistance with the GSH-GST modification and Dr. Yu-Ten Ju for his help in preparing the calmodulin-related constructs. This work was supported by the National Science Council of Taiwan under contract numbers NSC 97-2627-M-002-019 and NSC 97-2627-M-002-020. Technical support from NanoCore, the Core Facilities for Nanoscience and Nanotechnology at Academia Sinica, is also acknowledged.

1. Kenworthy AK (2001) Imaging protein-protein interactions using fluorescence resonance energy transfer microscopy. *Methods*, 24:289–296.
2. Sekar RB, Periasamy A (2003) Fluorescence resonance energy transfer (FRET) microscopy imaging of live cell protein localizations. *J Cell Biol*, 160:629–633.
3. Berggard T, Linse S, James P (2007) Methods for the detection and analysis of protein-protein interactions. *Proteomics*, 7:2833–2842.
4. Bunimovich YL, et al. (2006) Quantitative real-time measurements of DNA hybridization with alkylated nonoxidized silicon nanowires in electrolyte solution. *J Am Chem Soc*, 128:16323–16331.
5. Cui Y, Wei QQ, Park HK, Lieber CM (2001) Nanowire nanosensors for highly sensitive and selective detection of biological and chemical species. *Science*, 293:1289–1292.
6. Bi XY, Agarwal A, Balasubramanian N, Yang KL (2008) Tripeptide-modified silicon nanowire based field-effect transistors as real-time copper ion sensors. *Electrochem Commun*, 10:1868–1871.
7. Bi XY, et al. (2008) Development of electrochemical calcium sensors by using silicon nanowires modified with phosphotyrosine. *Biosens Bioelectron*, 23:1442–1448.
8. Zhang GJ, et al. (2008) DNA sensing by silicon nanowire: Charge layer distance dependence. *Nano Lett*, 8:1066–1070.
9. Patolsky F, et al. (2004) Electrical detection of single viruses. *P Nat Acad Sci USA*, 101:14017–14022.
10. Patolsky F, et al. (2006) Detection, stimulation, and inhibition of neuronal signals with high-density nanowire transistor arrays. *Science*, 313:1100–1104.
11. Zheng GF, Patolsky F, Cui Y, Wang WU, Lieber CM (2005) Multiplexed electrical detection of cancer markers with nanowire sensor arrays. *Nat Biotechnol*, 23:1294–1301.
12. Wang CW, et al. (2007) In situ detection of chromogranin a released from living neurons with a single-walled carbon-nanotube field-effect transistor. *Small*, 3:1350–1355.
13. Delves PJ, Roitt IM, Martin SJ, Burton DR (2006) *Roitt's essential immunology* 11th Ed (Blackwell Pub., Malden) 91.
14. Chin D, Means AR (2000) Calmodulin: a prototypical calcium sensor. *Trends Cell Biol*, 10:322–328.
15. Cheung WY (1980) Calmodulin plays a pivotal role in cellular-regulation. *Science*, 207:19–27.
16. Lin S-P, et al. (2009) A reversible surface functionalized nanowire transistor to study protein-protein interactions. *Nano Today*, 4:235–243.
17. Nishida M, et al. (1998) Three-dimensional structure of escherichia coli glutathione S-transferase complexed with glutathione sulfonate: Catalytic roles of Cys10 and His106. *J Mol Biol*, 281:135–147.
18. Seaton BA, Head JF, Engelman DM, Richards FM (1985) Calcium-induced increase in the radius of gyration and maximum dimension of calmodulin measured by small-angle X-ray scattering. *Biochemistry*, 24:6740–6743.
19. Creed GJ, Heydorn WE, Jacobowitz DM (1987) Observations and implications on the migration of calmodulin in a two-dimensional gel system. *Electrophoresis*, 8:251–252.
20. Stern E, et al. (2007) Importance of the Debye screening length on nanowire field effect transistor sensors. *Nano Lett*, 7:3405–3409.
21. Haiech J, Klee CB, Demaille JG (1981) Effects of cations on affinity of calmodulin for calcium: Ordered binding of calcium ions allows the specific activation of calmodulin-stimulated enzymes. Theoretical approach to study of multiple ligand binding to a macromolecule. *Biochemistry*, 20:3890–3897.
22. Haug A, Vitorello V (1996) Aluminum coordination to calmodulin: Thermodynamic and kinetic aspects. *Coord Chem Rev*, 149:113–124.
23. Wu AH (2004) The role of cardiac troponin in the recent redefinition of acute myocardial infraction. *Clin Lab Sci*, 17:50–52.
24. Keller CH, Olwin BB, Laporte DC, Storm DR (1982) Determination of the free-energy coupling for binding of calcium-ions and troponin-I to calmodulin. *Biochemistry*, 21:156–162.
25. LaPorte DC, Keller CH, Olwin BB, Storm DR (1981) Preparation of a fluorescent-labeled derivative of calmodulin which retains its affinity for calmodulin binding-proteins. *Biochemistry*, 20:3965–3972.
26. Bjellqvist B, et al. (1993) The focusing positions of polypeptides in immobilized pH gradients can be predicted from their amino-acid-sequences. *Electrophoresis*, 14:1023–1031.
27. Yao ZS, et al. (1999) The relationship of glycosylation and isoelectric point with tumor accumulation of avidin. *J Nucl Med*, 40:479–483.
28. Chao SH, Suzuki Y, Zysk JR, Cheung WY (1984) Activation of calmodulin by various metal-cations as a function of ionic radius. *Mol Pharmacol*, 26:75–82.
29. Kreye VA, Hofmann F, Muhleisen M (1986) Barium can replace calcium in calmodulin-dependent contractions of skinned renal-arteries of the rabbit. *Pflügers Arch*, 406:308–311.
30. Yamazaki J, Urushidani T, Nagao T (1996) Barium activates rat cerebellar nitric oxide synthase. *Jpn J Pharmacol*, 70:351–354.
31. Halling DB, Aracena-Parks P, Hamilton SL (2005) Regulation of voltage-gated Ca^{2+} channels by calmodulin. *Sci STKE*, 315:re15.
32. Liang HY, et al. (2003) Unified mechanisms of Ca^{2+} regulation across the Ca^{2+} channel family. *Neuron*, 39:951–960.
33. Cahill AL, Hurley JH, Fox AP (2000) Coexpression of cloned alpha(1B), beta(2a), and alpha(2)/delta subunits produces non-inactivating calcium currents similar to those found in bovine chromaffin cells. *J Neurosci*, 20:1685–1693.